JACS
JOURNAL OF THE AMERICAN CHEMICAL SOCIETY
Article
pubs.acs.org/JACS

Plasmon-Enhanced Photocatalytic CO_2 Conversion within Metal–Organic Frameworks under Visible Light

Kyung Min Choi,[†,§,⊥,#] Dohyung Kim,[‡,∥,#] Bunyarat Rungtaweevoranit,[†,§] Christopher A. Trickett,[†,§] Jesika Trese Deniz Barmanbek,[†] Ahmad S. Alshammari,[¶] Peidong Yang,*[,†,‡,□,∥] and Omar M. Yaghi*[,†,§,∥,¶]

[†]Department of Chemistry, [‡]Department of Materials Science and Engineering, and [∥]Kavli Energy NanoSciences Institute, University of California, Berkeley, California 94720, United States

[§]Materials Sciences Division, [□]Chemical Sciences Division, Lawrence Berkeley National Laboratory, Berkeley, California 94720, United States

[⊥]Department of Chemical and Biological Engineering, Sookmyung Women's University, Seoul 04310, Korea

[¶]King Abdulaziz City for Science and Technology, Post Office Box 6086, Riyadh 11442, Saudi Arabia

Supporting Information

ABSTRACT: Materials development for artificial photosynthesis, in particular, CO_2 reduction, has been under extensive efforts, ranging from inorganic semiconductors to molecular complexes. In this report, we demonstrate a metal–organic framework (MOF)-coated nanoparticle photocatalyst with enhanced CO_2 reduction activity and stability, which stems from having two different functional units for activity enhancement and catalytic stability combined together as a single construct. Covalently attaching a CO_2-to-CO conversion photocatalyst $Re^{I}(CO)_3(BPYDC)Cl$, BPYDC = 2,2′-bipyridine-5,5′-dicarboxylate, to a zirconium MOF, UiO-67 (Re_n-MOF), prevents dimerization leading to deactivation. By systematically controlling its density in the framework (n = 0, 1, 2, 3, 5, 11, 16, and 24 complexes per unit cell), the highest photocatalytic activity was found for Re_3-MOF. Structural analysis of Re_n-MOFs suggests that a fine balance of proximity between photoactive centers is needed for cooperatively enhanced photocatalytic activity, where an optimum number of Re complexes per unit cell should reach the highest activity. Based on the structure–activity correlation of Re_n-MOFs, Re_3-MOF was coated onto Ag nanocubes (Ag⊂Re_3-MOF), which spatially confined photoactive Re centers to the intensified near-surface electric fields at the surface of Ag nanocubes, resulting in a 7-fold enhancement of CO_2-to-CO conversion under visible light with long-term stability maintained up to 48 h.

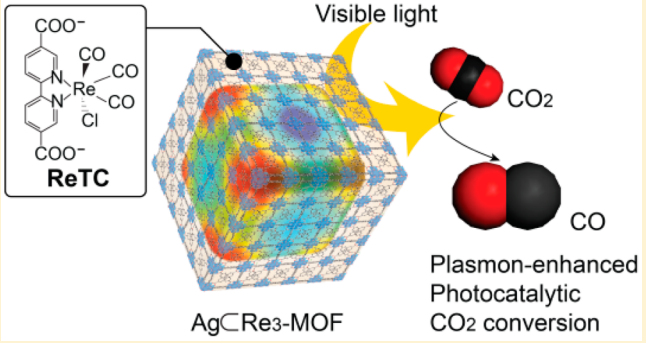

INTRODUCTION

Inorganic nanostructures and molecular complexes have been widely investigated as artificial photosynthetic catalysts.[1,2] The challenge is to find catalysts for carbon dioxide reduction with good activity, selectivity, and durability, especially under visible light. In this context, metal–organic frameworks (MOFs) offer many advantages because of the flexibility with which they can be designed and their pore environment varied.[3]

Here, we demonstrate how tunable photocatalytic activity can be realized by quantitatively and precisely controlling the density of covalently attached photoactive centers within the MOF interior and how this prevents the dimerization of the molecular catalyst and its deactivation. Furthermore, for the first time, these MOF catalytic units can be spatially localized within the enhanced electromagnetic field surrounding plasmonic silver nanocubes to significantly increase their photocatalytic activity for carbon dioxide conversion under visible light.[4] Specifically, we covalently attached $Re^{I}(CO)_3(BPYDC)(Cl)$, BPYDC = 2,2′-bipyridine-5,5′-dicarboxylate [hereafter referred to as ReTC], within a zirconium MOF based on the UiO-67-type structure[5] (hereafter, this Re-containing MOF is termed Re_n-MOF) and controlled its density in the pores in successive increments of n (n = 0, 1, 2, 3, 5, 11, 16, and 24 complexes per unit cell), finding the highest activity for n = 3 complexes. The effect of the molecular environment within MOFs for photocatalytic CO_2 reduction was studied, which provided further insights into the photocatalytic reaction pathway of the molecular Re complex. Placing this construct on silver nanocubes resulted in 7-fold enhancement of carbon dioxide photocatalytic conversion to carbon monoxide.

Many studies involving the use of photoactive metal complexes,[1,6] MOFs,[7,8] and inorganic nanostructures[9] for

Received: October 22, 2016
Published: November 26, 2016

DOI: 10.1021/jacs.6b11027
J. Am. Chem. Soc. 2017, 139, 356–362

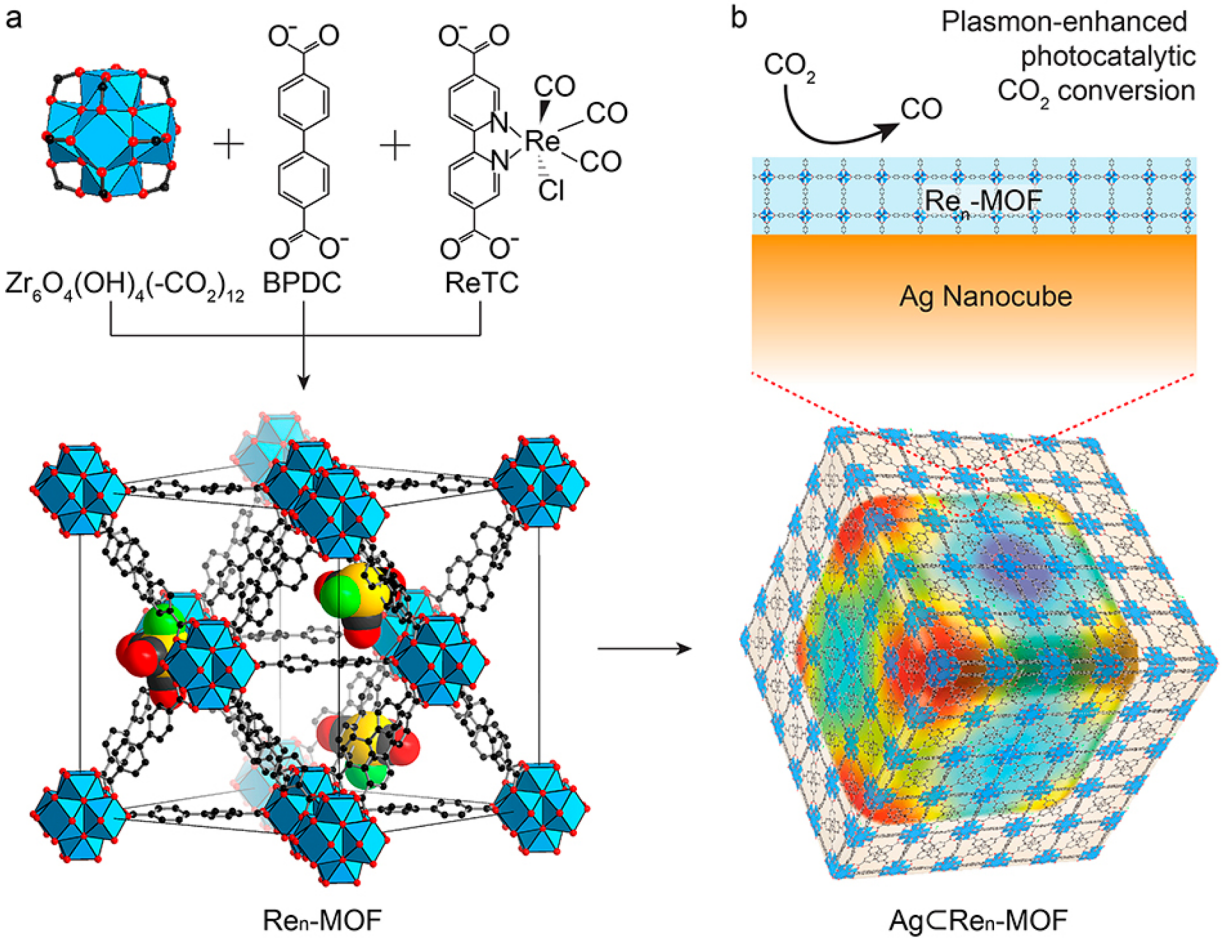

Figure 1. Structures of Re_n-MOF and Ag⊂Re_n-MOF for plasmon-enhanced photocatalytic CO_2 conversion. (a) $Zr_6O_4(OH)_4(-CO_2)_{12}$ secondary building units are combined with BPDC and ReTC linkers to form Re_n-MOF. The structure of Re_3-MOF identified from single-crystal X-ray diffraction is shown. The 12-coordinated Zr-based metal clusters are interconnected by 21 BPDC and 3 ReTC linkers in a face-centered cubic array. Atom labeling scheme: C, black; O, red; Zr, blue polyhedra; Re, yellow; Cl, green; H atoms are omitted for clarity. (b) Re_n-MOF coated on a Ag nanocube for enhanced photocatalytic conversion of CO_2.

carbon dioxide reduction have been reported with varying levels of performance. The present catalysts' unique performance is attributed to the precision and systematic variation applied in their design and the spatial resolution with which they can be interfaced with plasmonic nanostructures.

EXPERIMENTAL SECTION

Synthesis of $Re^{I}(CO)_3(H_2BPYDC)Cl$, H_2ReTC. $Re(CO)_5Cl$ (0.360 g, 1.000 mmol) and H_2BPYDC (0.240 g, 1.000 mmol) were added to methanol (100 mL). After the mixture was refluxed for 24 h under N_2, the resultant precipitate was filtered and the solvent was evaporated under reduced pressure to give the product. ^1H NMR (DMSO-d_6): δ 9.35 (s, 2H), 9.01 (d, 2H), 8.79 (d, 2H).

Synthesis of Re_n-MOFs. Different ratios of H_2ReTC and H_2BPDC (0, 5, 10, 20, 30, 50, 70, and 100 mol % of H_2ReTC, adding up to a total amount of 0.040 mmol of organic linker) were mixed with 10 mL of dimethylformamide (DMF) solution containing $ZrCl_4$ (9.320 mg, 0.040 mmol) and acetic acid (0.5 mL, 8.7 mmol) in a 20 mL vial, which was heated at 100 °C for 10 h. An orange precipitate was collected and washed three times with DMF using a centrifuge (9000 rpm for 10 min) and sonication and then sequentially immersed in anhydrous acetonitrile for three 24 h periods.

Synthesis of Ag Nanocubes. Silver nitrate (0.25 g) and copper(II) chloride (0.21 mg) were dissolved in 1,5-pentanediol (12.5 mL) in a 20 mL glass vial. In a separate vial, PVP (M_w = 55 000, 0.25 g) was dissolved in 1,5-pentanediol (12.5 mL). Using an oil bath, 1,5-pentanediol (20 mL) was heated for 10 min at 190 °C. Then the two precursor solutions were injected at different intervals: 500 μL of the silver nitrate solution every minute and 250 μL of the PVP solution every 30 s. The reaction was stopped once the solution turned opaque (~7 min).

Synthesis of Ag⊂Re_3-MOF. Ag nanocubes were washed three times with DMF using a centrifuge (9000 rpm for 10 min) and concentrated to a 3 mg/mL Ag nanocube solution. A Re-MOF stock solution was prepared by dissolving H_2BPDC (9.110 mg, 0.037 mmol), H_2ReTC (1.320 mg, 0.002 mmol), $ZrCl_4$ (9.32 mg, 0.04 mmol), and acetic acid (0.500 mL, 8.700 mmol) in 10 mL of DMF. Then 2.1 mL of the Re-MOF stock solution and 2 mL of the Ag nanocube solution were combined with 1 mL of DMF containing 0.125 mL of acetic acid in a 20 mL vial with a magnetic stirrer and heated at 90 °C in an aluminum heating block with vigorous stirring. The thickness of the Re-MOF layer could be controlled with reaction time; Ag⊂Re_3-MOF-16 nm and -33 nm were synthesized after 25 and 30 min, respectively. The precipitate was collected and washed three times with DMF using a centrifuge (9000 rpm for 10 min) and sonication and sequentially immersed in anhydrous acetonitrile for three 24 h periods.

Photocatalytic Experiments. The experiments were performed in a sealed batch-type custom cell. Samples were dispersed in acetonitrile (20 mL) with 1 mL of triethylamine added as a sacrificial electron donor. Initially, the cell was purged with CO_2 for 20 min and then sealed at 1 atm CO_2. A 300 W Xe lamp with visible band-pass filters was used so that the light contained regions in wavelengths

DOI: 10.1021/jacs.6b11027
J. Am. Chem. Soc. 2017, 139, 356−362

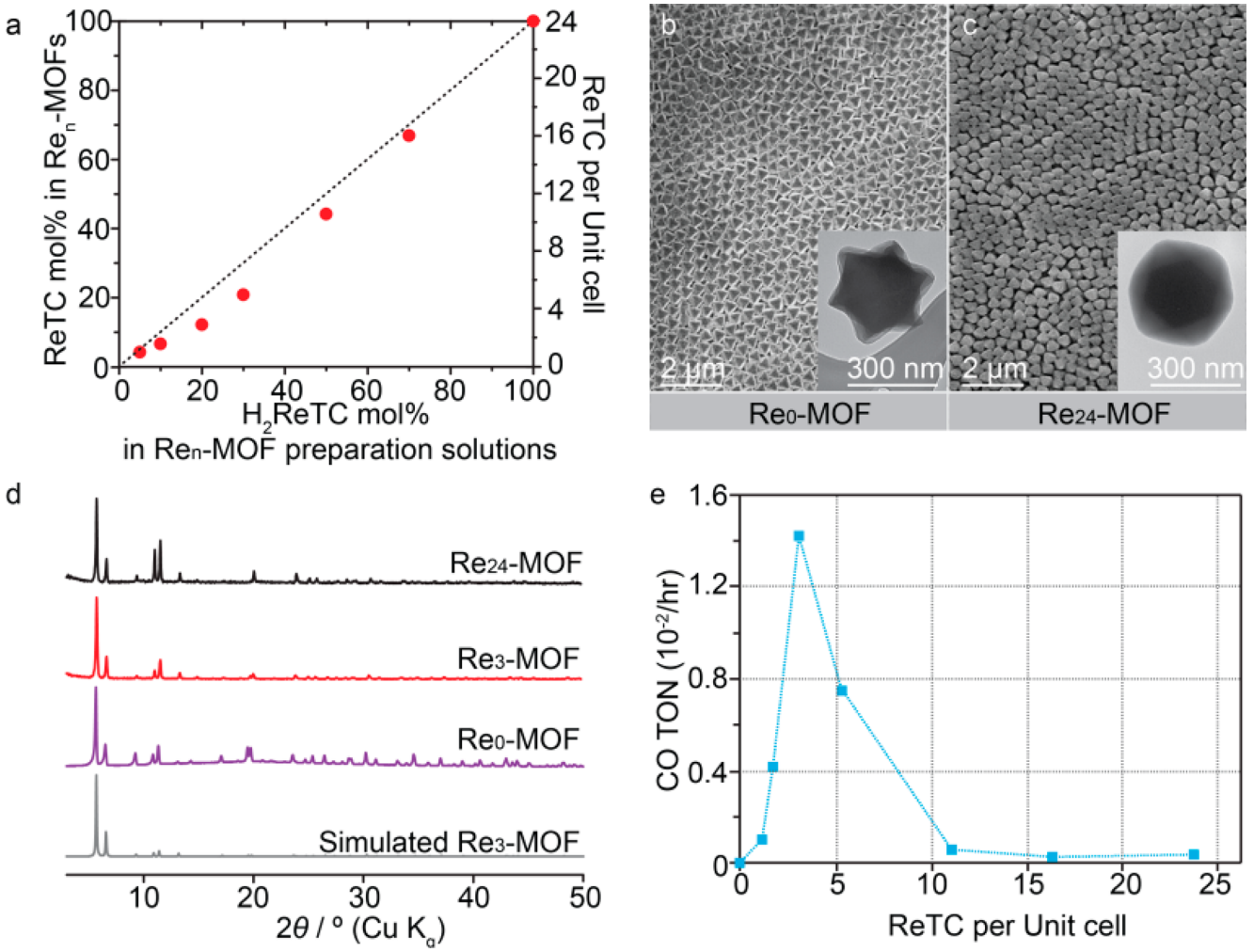

Figure 2. Characterization and photocatalytic activity of Re$_n$-MOFs. (a) Percent incorporation of ReTCs in Re$_n$-MOFs. SEM images of (b) Re$_0$- and (c) Re$_{24}$-MOFs. Insets are TEM images of each. (d) PXRD patterns of Re$_n$-MOFs in comparison with the simulated pattern of Re$_3$-MOF. (e) Photocatalytic CO_2-to-CO conversion activity under visible light (400−700 nm).

between 400 and 700 nm. The amount of Re tricarbonyl complex in each sample was 0.5−8 μmol, depending on the degree of ReTC incorporation inside MOFs, while the nanocrystal number per volume was kept similar. The products were measured by injecting 1 mL of gas in the headspace to a gas chromatograph (SRI) after every 1 or 2 h run.

Characterization. Powder X-ray diffraction patterns (PXRD) were recorded using a Bruker D8 Advance diffractometer (Göbel mirror monochromated Cu Kα radiation, λ = 1.54056 Å). Gas adsorption analysis was performed on a Quantachrome Quadrasorb-SI automatic volumetric gas adsorption analyzer. A liquid nitrogen bath (77 K) and ultrahigh purity grade N_2 and He (99.999%, Praxair) were used for the measurements. Samples were prepared and measured after being evacuated at 100 °C for 12 h. For transmission electron microscopy (TEM) observation, samples were first dispersed in an organic solvent by sonication and dropped onto a TEM grid. TEM was carried out at 200 kV using a JEOL JEM-2100. The amount of Re complexes in Re$_n$-MOFs was analyzed by an ICP−AES spectroscope (Optima 7000 DV, PerkinElmer). Samples (10 mg) were digested using a mixture of nitric acid (0.5 mL), hydrochloric acid (1.5 mL), and hydrofluoric acid (30 μL) and then diluted with 2 vol % of nitric acid solution (10 mL) before measurement. For NMR, 10 mg of dried sample was digested and dissolved by sonication in a mixture of DMSO-d_6 (1 mL), hydrofluoric acid (20 μL), and D_2O (20 μL). The digested solution was used directly for ^{1}H NMR. Attenuated total reflectance (ATR) Fourier transform infrared (FTIR) spectroscopy of neat samples was performed on a Bruker ALPHA platinum ATR-FTIR spectrometer equipped with a single reflection diamond ATR module. Liquid samples were measured by placing a sample droplet on the sample stage covered with a cap for preventing solvent evaporation.

RESULTS AND DISCUSSION

Structural Analysis and Photocatalytic Activity of Re$_n$-MOFs. *Structural Analysis of Re$_3$-MOF.* The structural determination of Re$_3$-MOF was carried out by single-crystal X-ray diffraction (Figure 1). Single crystals of Re$_3$-MOF were prepared by dissolving the protonated form of H_2ReTC (20 mol %), H_2BPDC (80 mol %, BPDC = 4,4′-biphenyldicarboxylate), and $ZrOCl_2·8H_2O$ in a solution mixture of DEF/formic acid in a 20 mL screw-capped vial and heating at 140 °C for 12 h [Figure S1 in Supporting Information (SI)]. The analysis of single-crystal X-ray diffraction data reveals that Re$_3$-MOF crystallizes in the cubic $Fm\bar{3}m$ space group with a unit cell parameter a = 26.7213(8) Å (Table S1 and Figure S2). Each Zr secondary building unit, $Zr_6O_4(OH)_4(-CO_2)_{12}$, is coordinated to a total of 12 linkers (ReTC and BPDC), resulting in a three-dimensional fcu network. Inductively coupled plasma atomic emission spectroscopy (ICP-AES) analysis performed on these crystals gave a molar ratio of 0.12 mol of Re to 1 mol Zr. This corresponds to 3 ReTCs per unit cell (i.e., Re$_3$-MOF), as confirmed by the X-ray structure of single-crystalline

DOI: 10.1021/jacs.6b11027
J. Am. Chem. Soc. 2017, 139, 356−362

$Zr_6O_4(OH)_4[Re(CO)_3(Cl)\text{-}BPYDC]_{0.72}(BPDC)_{5.28}$, where covalently bound ReTCs are found in octahedral cavities of face-centered cubic arrangement. Moreover, chloride occupies the axial position and was refined from the Fourier difference map, indicating *fac*-arrangement of the ReTC in Re_3-MOF, which is an identical geometry compared to that of the mononuclear Re complex in solution[10] (Figure S2 in SI).

The *fac*-arrangement of ReTC in Re_3-MOF is also supported by infrared (IR) spectroscopy (Figure S3 in SI), ultraviolet−visible (UV−vis) spectroscopy (Figure S4 in SI), and ^1H nuclear magnetic resonance (NMR) spectra (Figure S5 in SI). The IR spectrum of Re_3-MOF was measured in powder form, and ν(CO) bands were observed at 2022, 1920, and 1910 cm^{-1} (Figure S3 in SI), consistent with the *fac*-isomer of molecular ReTC.[10] The UV−vis spectrum, measured as a powder mixed with KBr, has a metal-to-ligand charge transfer (MLCT) absorption band at 400 nm, indicative of the *fac*-isomer of ReTC[10] (Figure S4 in SI). The amount of ReTC in the MOF and its molecular configuration were further confirmed from ^1H NMR of a HF-digested solution of Re_3-MOF (Figure S5 in SI).

ReTC Density Varied in Re_n-MOFs. To examine how the amount of ReTC in MOFs affects the structural environment within the MOF interior for CO_2 catalytic turnover, the ReTC density was varied in the range from Re_0-MOF (ReTC free MOF) to Re_{24}-MOF (ReTC at maximal loading). This was done by adding increasing amounts of H_2ReTC to the total amount of organic linkers during MOF synthesis, which resulted in Re_n-MOFs (n = 0, 1, 2, 3, 5, 11, 16, and 24) identified from ICP-AES (Figure 2a). All samples were synthesized as monocrystalline nanoparticles (Figures S6−S8 in SI) as this may facilitate diffusion of substrates and products to and from the active Re catalytic centers. Representative scanning electron microscopy (SEM) images (Figure 2b,c and Figure S7 in SI) of Re_n-MOFs show great size uniformity (ca. 300 nm) and identical octahedral geometry of particles regardless of the amount of ReTC incorporated. The crystallinity of Re_n-MOFs was examined by PXRD (Figure 2d and Figure S8 in SI), which gave sharp diffraction lines matching those of the simulated pattern obtained from experimental single-crystal X-ray diffraction data of Re_3-MOF. This clearly indicates preservation of the single-crystalline Re_3-MOF structure upon introduction of different density of ReTC in Re_n-MOFs. The permanent porosity of all Re_n-MOF samples was confirmed by measurement of their N_2 sorption isotherms (Figure S9 in SI). UV−vis spectroscopy for all Re_n-MOFs showed that the MLCT absorption band intensities increase as more ReTCs are incorporated into the framework, further confirming the varied density of the photoactive units in Re_n-MOFs (Figure S10 in SI).

Photocatalytic CO_2 Conversion for Re_n-MOFs. All Re_n-MOFs used for photocatalytic CO_2 conversion were dispersed in an acetonitrile/triethylamine mixture (MeCN/TEA = 20:1) saturated with CO_2, where TEA served as a sacrificial electron donor. Measurements were conducted under visible light (300 W Xe lamp, visible band-pass = 400−700 nm) to utilize the visible light absorption feature of ReTC. We note this is in contrast to previous work where it relied on the intense absorption at the UV region (300−350 nm) associated with $\pi-\pi^*$ energy transition of the bipyridine linker.[7] The products were analyzed and quantified using gas chromatography and normalized to the number of ReTC in Re_n-MOFs to get the turnover number (TON). Photocatalytic CO_2-to-CO conversion behavior of Re_n-MOFs is shown in Figure 2e, reaching peak activity with Re_3-MOF. In the absence of CO_2 (under Ar atmosphere) or with no ReTC, there was no CO generation observed. The performance of Re_n-MOFs was stable at least up to 4 h (Figure S11 in SI) compared to the molecular counterpart,[11] which deactivates within the first hour (Figure S12 in SI). The enhanced stability of Re_n-MOFs is from the covalent attachment of Re centers in ReTC, which prevents the prevailing deactivation pathway of dimerization commonly observed with photoactive molecular complexes (Figures S13 and S14 in SI). IR spectra of Re_3-MOF before and after the reaction (Figure S15 in SI) show that Re_n-MOFs preserve the molecular configuration of *fac*-ReTC after photocatalysis, while, in comparison, the ν(CO) bands for molecular H_2ReTC are shifted because of dimerization. This clearly indicates the inability of ReTC to dimerize due to its covalent bonding to the MOF in Re_n-MOFs.

Effect of the Molecular Environment within MOFs for Photocatalytic CO_2 Reduction. *IR Spectroscopy of Re_n-MOFs and Molecular H_2ReTC.* The photocatalytic trend observed for Re_n-MOFs should be closely related to the configuration of ReTC and its surrounding environment. The vibrational stretching modes of ReTC carbonyl ligands in Re_n-MOFs were probed by IR spectroscopy and compared with those of the molecular H_2ReTC (Figure 3). In the cases of Re_1-, Re_2-, and Re_3-MOFs, ν(CO) bands were observed at 2022, 1920, and 1910 cm^{-1}, which are identical to the IR spectra of H_2ReTC dispersed in solution. On the other hand, the ν(CO) bands at lower wavenumbers were shifted to lower frequency for Re_5-, Re_{11}-, Re_{16}-, and Re_{24}-MOFs. This indicated that there is electron back-donation to the carbonyl ligand from Re of other ReTCs, weakening the CO bond strength.[12] This effect is possibly due to weak interactions between contiguous overlapping ReTCs. This was also observed when H_2ReTC molecules are tightly packed as powder and moistened with acetonitrile, where ν(CO) bands are shifted to 1900 and 1880 cm^{-1}.

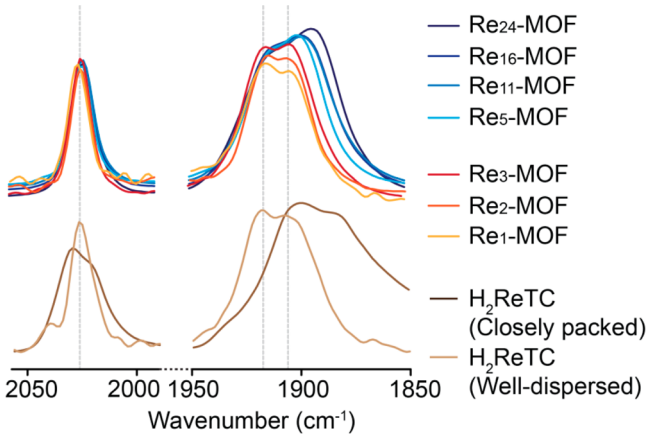

Figure 3. IR spectra of Re_n-MOFs and H_2ReTC.

Re_n-MOFs with n Greater than 4. Considering that ReTCs are observed within the octahedral cavity of Re_3-MOF from single-crystal X-ray diffraction and the axial rotation of the ReTC linker backbone, the maximum number of ReTC units that can be incorporated into Re_n-MOF without overlapping is 4 per unit cell, with each octahedral cavity being occupied with a single ReTC complex (Figure S16 in SI). We believe a statistically variable distribution of ReTCs within the frame-

DOI: 10.1021/jacs.6b11027
J. Am. Chem. Soc. 2017, 139, 356−362

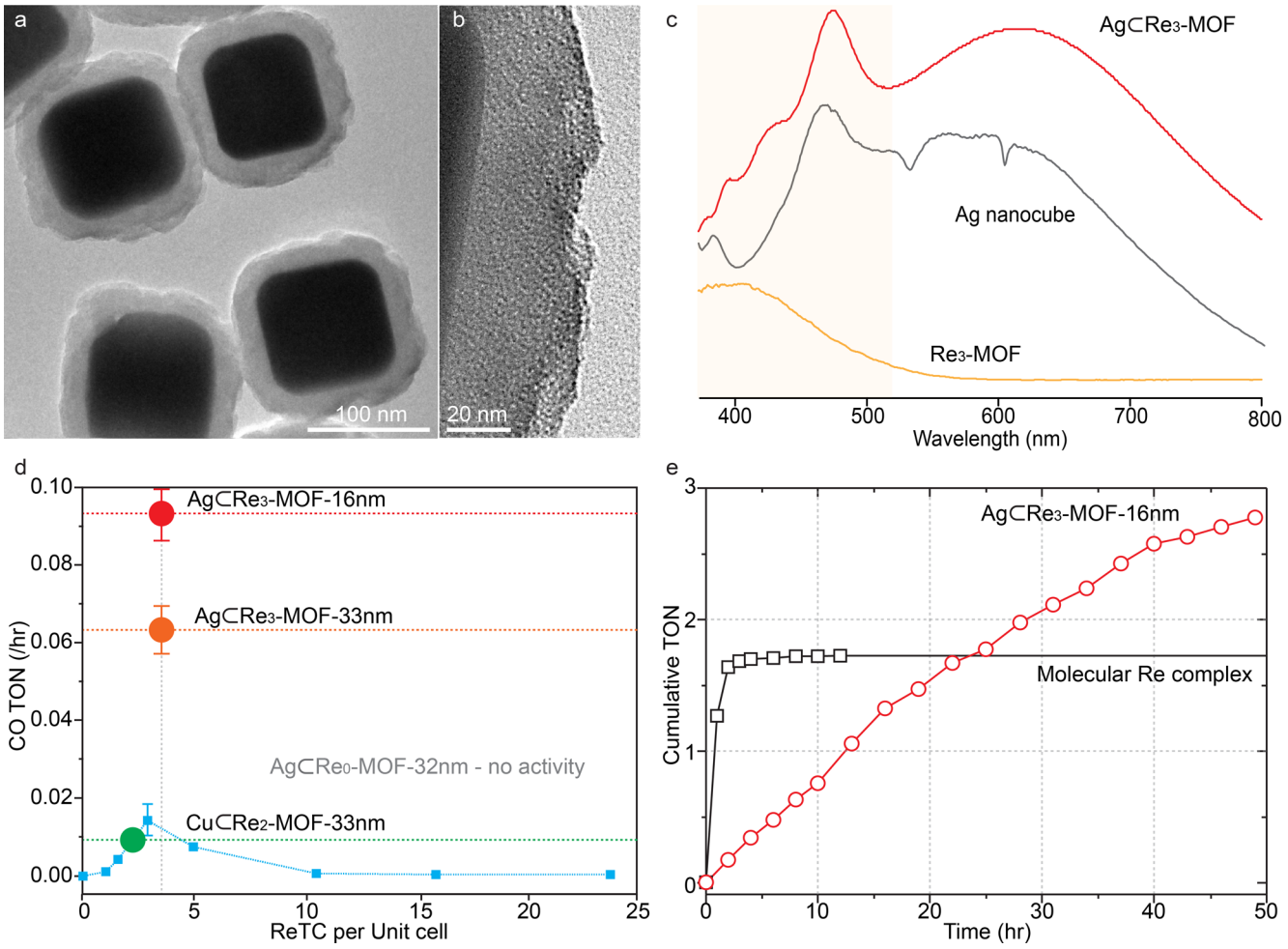

Figure 4. Characterization of AgCRe$_3$-MOF. (a) TEM image of AgCRe$_3$-MOF showing Re$_3$-MOF constructed on the surface of a Ag nanocube. (b) Magnified image of Re$_3$-MOF. (c) UV−vis spectra of Re$_3$-MOF, Ag nanocube, and AgCRe$_3$-MOF. (d) Photocatalytic CO_2-to-CO conversion activity of Re$_n$-MOFs (blue line), AgCRe$_0$-MOF, CuCRe$_2$-MOF, and AgCRe$_3$-MOFs with MOF thickness of 16 and 33 nm. (e) Stable performance of AgCRe$_3$-MOF compared to molecular H_2ReTC.

work is most reasonable to expect. Beyond this point, the likelihood of ReTCs occupying adjacent linkers and hence overlapping increases. Indeed, if the linkers can rotate 180° into adjacent octahedral cavities, beyond 4 per unit cell, there will unavoidably be some ReTCs clashing from this rotation (Figure S17a in SI). The IR spectra are consistent with the unit cell structure considerations where Re$_5$-MOF is just beyond the limit of ReTC being undisturbed. Therefore, the excessive occupation of ReTCs in Re$_n$-MOFs appear to cause a change in their vibrational state,[13] which may not be favorable for reducing CO_2 and decreases activity for Re$_n$-MOFs with n greater than 4. Another aspect to note is the accessible pore volume of Re$_n$-MOFs: N_2 uptake on a volumetric scale (Figure S9 in SI) is lower for frameworks with more than 4 ReTC per unit cell. This indicates that substrate and product diffusion may also be limited within Re$_n$-MOFs with n greater than 4, further resulting in the observed lowering of activity.

Re$_n$-MOFs with n Less than 4. However, we see an increase in activity in the lower regime of ReTC incorporation, from Re$_1$ to Re$_3$. Though a unimolecular pathway has been reported to exist for molecular ReTC,[14a] the observed rise in photocatalytic activity with more ReTC units within Re$_n$-MOF (n < 4) implies that the bimolecular reaction pathway (bridging or outer-sphere electron transfer) is the source of the higher turnover,[13,14] which is expected for a reaction involving 2 electrons (Figures S17b and 18 in SI). Therefore, a fine balance of proximity between photoactive centers is needed for such cooperatively enhanced activity. Furthermore, reduced activity compared to the molecular ReTC in solution (Figures S11 and S12 in SI) indicates that restricting the free motion of the molecular complex may limit its activity though it is protected from rapid deactivation. The present study of Re$_n$-MOFs not only elucidates the effect of the molecular environment within MOFs for photocatalytic CO_2 reduction but also provides further insights into the photocatalytic reaction pathway of molecular ReTC.

Plasmon-Enhanced Photocatalytic Activity of Re$_n$-MOFs. *Synthesis and Characterization of Re$_n$-MOFs Coated on Plasmonic Ag Nanocubes.* Coupling Re$_3$-MOF to a plasmonic Ag nanoparticle was performed to demonstrate an effective strategy in creating a bifunctional catalyst with enhanced activity and long-term stability. The optimal Re$_3$-MOF structure with the highest turnover was coated on Ag nanocubes (AgCRe$_3$-MOF). Once irradiated with light, the Ag nanocubes generate intensified near-surface electric fields at their surface plasmon resonance frequency that can be orders of magnitude higher in intensity than the incident electromagnetic field[4b,15] Therefore, it is expected that Re$_3$-MOF coating on the

DOI: 10.1021/jacs.6b11027
J. Am. Chem. Soc. 2017, 139, 356−362

Ag nanocubes can spatially localize photoactive Re centers to the intensified electric fields with enhanced photocatalytic activity. More recently, there have been some examples of combining metal nanoparticles with MOFs capable of catalysis that led to enhancement in their performance.[16] Ag nanocubes prepared by the polyol process[17] were used in the synthesis procedure of Re_n-MOF to give Ag⊂Re_3-MOF. Figure 4a shows a TEM image of Ag⊂Re_3-MOF. The dark area in the core is the Ag nanocube (98 nm in size), and the brighter outer part is the Re_3-MOF with a thickness of 33 nm. The magnified image of the outer part (Figure 4b) shows lattice fringes from the crystalline Re_3-MOF layer. ICP-AES analysis revealed that the Re_3-MOF layer contains the expected three ReTCs per unit cell. The crystallinity of Ag⊂Re_3-MOF was examined by PXRD (Figure S19 in SI). The resulting diffraction lines of Ag⊂Re_3-MOF match those of Ag and Re_3-MOF, indicating the preservation of the Ag metallic phase and the formation of the Re_3-MOF structure on the surface of Ag. The permanent porosity of Ag⊂Re_3-MOF was confirmed by N_2 sorption (Figure S20 in SI). IR spectroscopy showed that ν(CO) bands were consistent with those of molecular H_2ReTC and Re_3-MOF (Figure S21 in SI). From the UV−vis spectrum (Figure 4c), the Ag nanocube exhibits a strong quadrupolar localized surface plasmon resonance (LSPR) scattering peak ($\lambda_{max} \sim 480$ nm),[17,18] which overlaps with the absorption range of ReTC (400 nm < λ < 550 nm) in the visible region. Furthermore, the Ag⊂Re_3-MOF structure retains the characteristic LSPR features of the Ag core after being coated with the Re_3-MOF. Therefore, it is expected that the intensified near-field created at the surface of Ag nanocubes can be absorbed by ReTCs incorporated into the Re_3-MOF layer for photocatalytic enhancement.

Photocatalytic Activity and Stability of Ag⊂Re_n-MOFs. Photocatalytic CO_2-to-CO conversion activity of Ag⊂Re_3-MOF was performed under conditions identical to those expressed above (Figure 4d). As expected, Ag⊂Re_3-MOF exhibits 5-fold enhancement of activity over Re_3-MOF under visible light. Since the intensity of the near-field from LSPR decays exponentially with the distance from the surface of the nanoparticle,[4d] ReTCs in a thinner MOF layer will be under the influence of a stronger electric field on average, leading to superior turnover. A thinner Re_3-MOF layer (16 nm) was coated on Ag nanocubes by controlling the synthetic conditions (Figure S22 in SI), and this structure provided 7-fold enhancement of photocatalytic activity (Figure 4d). When there was no ReTC in the MOF layer (i.e., Ag⊂Re_0-MOF) (Figure S23 in SI), there was no activity observed, ruling out the possibility of Ag being responsible for CO production. Additionally, when Re_2-MOF was coated on Cu nanoparticles of similar size (~100 nm, Figure S24 in SI), activity enhancement was not observed (Figure 4d) as the Cu nanoparticles do not have LSPR characteristics that match the absorption features of ReTC (Figure S25 in SI).

The Ag nanocube coated with Re-MOF should exhibit not only enhanced photocatalytic activity but long-term stability as well from having ReTCs covalently bound within the MOF. The stability of the Ag⊂Re_3-MOF structure was tested by measuring its activity up to 48 h under visible light (Figure 4e). Compared to molecular H_2ReTC, which rapidly deactivates within the first hour possibly from dimerization as previously reported,[11] Ag⊂Re_3-MOF shows stable photocatalytic performance throughout the entire period, and its cumulative TON exceeds that of H_2ReTC after 24 h. The stability of the structure was confirmed with TEM and IR spectroscopy following the long-term measurement (Figures S26 and S27 in SI). The CO produced from Ag⊂Re_3-MOF almost doubled from that of H_2ReTC after 48 h, demonstrating the combined effects gained from this bifunctional catalyst construct.

SUMMARY

We show how covalently attached photoactive centers within MOF interior can be spatially localized and subjected to the enhanced electromagnetic field surrounding plasmonic silver nanocubes to significantly increase their photocatalytic activity. We covalently attached $Re^{I}(CO)_3$(BPYDC)Cl, BPYDC = 2,2′-bipyridine-5,5′-dicarboxylate, into a zirconium MOF, UiO-67, and controlled its density in the pores in increments (0, 1, 2, 3, 5, 11, 16, and 24 complexes per unit cell), which led to observing the highest activity for three complexes. This activity trend resulted from the molecular environment within MOFs that varied with ReTC density. Placing the optimal Re_3-MOF structure with the highest turnover on silver nanocubes resulted in 7-fold enhancement of photocatalytic activity under visible light.

ASSOCIATED CONTENT

Supporting Information

The Supporting Information is available free of charge on the ACS Publications website at DOI: 10.1021/jacs.6b11027.

Materials and methods, structural analysis of single-crystalline Re_3-MOF, and additional characterization of Re_n-MOF and Ag⊂Re_3-MOF (PDF)

X-ray data for Re_3-MOF (CIF)

AUTHOR INFORMATION

Corresponding Authors

*p_yang@berkeley.edu

*yaghi@berkeley.edu

Author Contributions

#K.M.C. and D.K. contributed equally.

Notes

The authors declare no competing financial interest.

ACKNOWLEDGMENTS

The research performed in the O.M.Y. laboratory was supported by BASF SE (Ludwigshafen, Germany) and King Abdulaziz City for Science and Technology as part of a joint KACST−UC Berkeley collaboration (Center of Excellence for Nanomaterials and Clean Energy Applications). Financial support for part of this work performed in the P.Y. laboratory was supported by the Director, Office of Science, Office of Basic Energy Sciences, Chemical Sciences, Geosciences, & Biosciences Division, of the U.S. Department of Energy under Contract No. DE-AC02-05CH11231, FWP No. CH030201 (Catalysis Research Program). D.K. acknowledges support from Samsung Scholarship, and K.M.C. acknowledges support from Basic Science Research Program through the National Research Foundation of Korea (NRF) (2016R1C1B1010781) and Sookmyung Women's University Research Grant (1-1603-2038). Work performed at the Advanced Light Source is supported by the Director, Office of Science, Office of Basic Energy Sciences, of the U.S. Department of Energy under Contract No. DE-AC02-05CH11231. The NMR work at the Molecular Foundry was supported by the Office of Science,

DOI: 10.1021/jacs.6b11027
J. Am. Chem. Soc. 2017, 139, 356−362

Office of Basic Energy Sciences, of the U.S. Department of Energy under Contract No. DE-AC02-05CH11231. We thank Chenlu Xie and Dr. Tsung Rong for help in the synthesis of Ag nanocubes, and Drs. Wooyeol Kim and Heinz Frei for the use of IR and UV−vis instruments. Drs. S. Teat and K. Gagnon are acknowledged for the synchrotron X-ray diffraction data acquisition support at the beamline 11.3.1 at Advanced Light Source, Lawrence Berkeley National Laboratory.

REFERENCES

(1) (a) White, J. L.; Baruch, M. F.; Pander, J. E., III; Hu, Y.; Fortmeyer, I. C.; Park, J. E.; Zhang, T.; Liao, K.; Gu, J.; Yan, Y.; Shaw, T. W.; Abelev, E.; Bocarsly, A. B. *Chem. Rev.* **2015**, *115*, 12888. (b) Berardi, S.; Drouet, S.; Francàs, L.; Gimbert-Suriñach, C.; Guttentag, M.; Richmond, C.; Stoll, T.; Llobet, A. *Chem. Soc. Rev.* **2014**, *43*, 7501.

(2) (a) Kim, D.; Sakimoto, K. K.; Hong, D.; Yang, P. *Angew. Chem., Int. Ed.* **2015**, *54*, 3259. (b) Kumar, B.; Llorente, M.; Froehlich, J.; Dang, T.; Sathrum, A.; Kubiak, C. P. *Annu. Rev. Phys. Chem.* **2012**, *63*, 541.

(3) Furukawa, H.; Cordova, K. E.; O'Keeffe, M.; Yaghi, O. M. *Science* **2013**, *341*, 974.

(4) (a) Hou, W.; Hung, W. H.; Pavaskar, P.; Goeppert, A.; Aykol, M.; Cronin, S. B. *ACS Catal.* **2011**, *1*, 929. (b) Hou, W.; Cronin, S. B. *Adv. Funct. Mater.* **2013**, *23*, 1612. (c) Tu, W.; Zhou, Y.; Li, H.; Li, P.; Zou, Z. *Nanoscale* **2015**, *7*, 14232. (d) Yuan, Y.-P.; Ruan, L.-W.; Barber, J.; Loo, S. C. J.; Xue, C. *Energy Environ. Sci.* **2014**, *7*, 3934.

(5) Cavka, J. H.; Jakobsen, S.; Olsbye, U.; Guillou, N.; Lamberti, C.; Bordiga, S.; Lillerud, K. P. *J. Am. Chem. Soc.* **2008**, *130*, 13850.

(6) (a) Smieja, J. M.; Benson, E. E.; Kumar, B.; Grice, K. A.; Seu, C. S.; Miller, A. J. M.; Mayer, J. M.; Kubiak, C. P. *Proc. Natl. Acad. Sci. U. S. A.* **2012**, *109*, 15646. (b) Morris, A. J.; Meyer, G. J.; Fujita, E. *Acc. Chem. Res.* **2009**, *42*, 1983.

(7) (a) Wang, C.; Xie, Z.; deKrafft, K. E.; Lin, W. *J. Am. Chem. Soc.* **2011**, *133*, 13445. (b) Blake, A. J.; Champness, N. R.; Easun, T. L.; Allan, D. R.; Nowell, H.; George, M. W.; Jia, J.; Sun, X.-Z. *Nat. Chem.* **2010**, *2*, 688. (c) Zhang, T.; Lin, W. *Chem. Soc. Rev.* **2014**, *43*, 5982. (d) Wang, J.-L.; Wang, C.; Lin, W. *ACS Catal.* **2012**, *2*, 2630.

(8) (a) Chambers, M. B.; Wang, X.; Elgrishi, N.; Hendon, C. H.; Walsh, A.; Bonnefoy, J.; Canivet, J.; Quadrelli, E. A.; Farrusseng, D.; Mellot-Draznieks, C.; Fontecave, M. *ChemSusChem* **2015**, *8*, 603. (b) Lee, Y.; Kim, S.; Kang, J. K.; Cohen, S. M. *Chem. Commun.* **2015**, *51*, 5735. (c) Fei, H.; Sampson, M. D.; Lee, Y.; Kubiak, C. P.; Cohen, S. M. *Inorg. Chem.* **2015**, *54*, 6821. (d) Fu, Y.; Sun, D.; Chen, Y.; Huang, R.; Ding, Z.; Fu, X.; Li, Z. *Angew. Chem., Int. Ed.* **2012**, *51*, 3364. (e) Wang, D.; Huang, R.; Liu, W.; Sun, D.; Li, Z. *ACS Catal.* **2014**, *4*, 4254. (f) Wang, S.; Yao, W.; Lin, J.; Ding, Z.; Wang, X. *Angew. Chem., Int. Ed.* **2014**, *53*, 1034. (g) Huang, R.; Peng, Y.; Wang, C.; Shi, Z.; Lin, W. *Eur. J. Inorg. Chem.* **2016**, *2016*, 4358. (h) Easun, T. L.; Jia, J.; Calladine, J. A.; Blackmore, D. L.; Stapleton, C. S.; Vuong, K. Q.; Champness, N. R.; George, M. W. *Inorg. Chem.* **2014**, *53*, 2606. (i) Hod, I.; Sampson, M. D.; Deria, P.; Kubiak, C. P.; Farha, O. K.; Hupp, J. T. *ACS Catal.* **2015**, *5*, 6302.

(9) (a) Liang, Y. T.; Vijayan, B. K.; Gray, K. A.; Hersam, M. C. *Nano Lett.* **2011**, *11*, 2865. (b) Neaţu, Ş.; Maciá-Agulló, J. A.; Concepción, P.; Garcia, H. *J. Am. Chem. Soc.* **2014**, *136*, 15969. (c) Ma, Y.; Wang, X.; Jia, Y.; Chen, X.; Han, H.; Li, C. *Chem. Rev.* **2014**, *114*, 9987. (d) Liang, W.; Church, T. L.; Zheng, S.; Zhou, C.; Haynes, B. S.; D'Alessandro, D. M. *Chem. - Eur. J.* **2015**, *21*, 18576.

(10) Sato, S.; Morimoto, T.; Ishitani, O. *Inorg. Chem.* **2007**, *46*, 9051.

(11) Benson, E. E.; Kubiak, C. P. *Chem. Commun.* **2012**, *48*, 7374.

(12) Zhao, H. C.; Mello, B.; Fu, B. L.; Chowdhury, H.; Szalda, D. J.; Tsai, M. K.; Grills, D. C.; Rochford, J. *Organometallics* **2013**, *32*, 1832.

(13) Hayashi, Y.; Kita, S.; Brunschwig, B. S.; Fujita, E. *J. Am. Chem. Soc.* **2003**, *125*, 11976.

(14) (a) Gibson, D. H.; Yin, X.; He, H.; Mashuta, M. S. *Organometallics* **2003**, *22*, 337. (b) Gibson, D. H.; Yin, X. *J. Am. Chem. Soc.* **1998**, *120*, 11200. (c) Takeda, H.; Koike, K.; Inoue, H.; Ishitani, O. *J. Am. Chem. Soc.* **2008**, *130*, 2023. (d) Meister, S.; Reithmeier, R. O.; Tschurl, M.; Heiz, U.; Rieger, B. *ChemCatChem* **2015**, *7*, 690.

(15) (a) Linic, S.; Christopher, P.; Ingram, D. B. *Nat. Mater.* **2011**, *10*, 911. (b) Jeong, N. C.; Prasittichai, C.; Hupp, J. T. *Langmuir* **2011**, *27*, 14609.

(16) (a) Yuan, X.; Wang, H.; Wu, Y.; Zeng, G.; Chen, X.; Leng, L.; Wu, Z.; Li, H. *Appl. Organomet. Chem.* **2016**, *30*, 289. (b) Gu, Z.; Chen, L.; Duan, B.; Luo, Q.; Liu, J.; Duan, C. *Chem. Commun.* **2016**, *52*, 116. (c) Gao, S.-T.; Liu, W.-H.; Shang, N.-Z.; Feng, C.; Wu, Q.-H.; Wang, Z.; Wang, C. *RSC Adv.* **2014**, *4*, 61736. (d) Hu, P.; Morabito, J. V.; Tsung, C.-K. *ACS Catal.* **2014**, *4*, 4409. (e) Hu, P.; Zhuang, J.; Chou, L.-Y.; Lee, H. K.; Ling, X. Y.; Chuang, Y.-C.; Tsung, C.-K. *J. Am. Chem. Soc.* **2014**, *136*, 10561.

(17) Tao, A.; Sinsermsuksakul, P.; Yang, P. *Angew. Chem., Int. Ed.* **2006**, *45*, 4597.

(18) Wu, H.-J.; Henzie, J.; Lin, W.-C.; Rhodes, C.; Li, Z.; Sartorel, E.; Thorner, J.; Yang, P.; Groves, J. T. *Nat. Methods* **2012**, *9*, 1189.

DOI: 10.1021/jacs.6b11027
J. Am. Chem. Soc. 2017, 139, 356−362